# Investigating impact demagnetization through laser impacts and SQUID microscopy

Jérôme Gattacceca CEREGE, CNRS/Université Aix-Marseille 3, France
Michel Boustie Laboratoire de Combustion et Détonique, CNRS/ENSMA, Poitiers, France
Benjamin P. Weiss Massachusetts Institute of Technology, 77 Massachusetts Avenue, Cambridge, Massachusetts 02139, USA
Pierre Rochette CEREGE, CNRS/Université Aix-Marseille 3, France
Eduardo A. Lima
Luis E. Fong
Franz J. Baudenbacher
Vanderbilt University, 2201 West End Avenue, Nashville, Tennessee 37235, USA

## ABSTRACT

**Understanding demagnetization by hypervelocity impacts is crucial for the interpretation of planetary magnetic anomalies and remanent magnetization in meteorites. We describe an innovative approach for investigating the effects of impacts on the remanent magnetization of geologic materials. It consists of the combination of pulsed laser impacts and Superconducting Quantum Interference Device (SQUID) microscopy. Laser impacts are nondestructive, create shocks with peak pressures as high as several hundred GPa, and allow well-calibrated modeling of shock wave propagation within the impacted samples. High-resolution SQUID microscopy quantitatively maps the magnetic field of room-temperature samples with an unprecedented spatial resolution of ~100 μm. We present shock modeling and magnetic field data obtained for two laser impacts on a magnetite-bearing basalt sample. Magnetic measurements show a demagnetized area at the impact locations. We also show that high-resolution magnetic measurements combined with impact modeling provide a continuous relation between the demagnetization intensity and the peak pressure undergone by the sample. This promising technique will allow for the investigation of the demagnetization behavior of a variety of geological materials upon impacts, with implications for our understanding of the magnetization of extraterrestrial materials and of terrestrial impact structures.**

**Keywords:** impact demagnetization, SQUID microscopy, laser impact, magnetite.

## INTRODUCTION

Hypervelocity impacts are phenomena of major importance for the evolution of the solid bodies of the solar system. In particular, they may play a crucial role in the magnetic records of many extraterrestrial bodies. Impact demagnetization is invoked to explain specific features of the crustal magnetization of Mars (Hood et al., 2003), the Moon (Halekas et al., 2003), and asteroids (Chen et al., 1995).

In the 1970s, the complex magnetization observed in the Apollo samples triggered the study of the effect of impacts on remanent magnetization (Cisowski et al., 1976; Martelli and Newton, 1977; Fuller, 1977; Cisowski and Fuller, 1978; Srnka et al., 1979). Experimental efforts were mainly devoted to FeNi alloys, the dominant magnetic minerals in lunar samples and most meteorites. The magnetic properties of FeNi were investigated up to pressures of 80 GPa (Wasilewski, 1976; Dickinson and Wasilewski, 2000). Magnetite, in view of its importance in the understanding of the magnetic signature of terrestrial and possibly Martian impacts, was studied at impact pressures up to 1 GPa (Pohl et al., 1975) and static pressures up to 5 GPa (Gilder et al., 2002, 2004). The magnetism of hematite and nontronite, two other candidate Martian dust minerals, has been investigated to peak shock pressures of 27 and 32 GPa, respectively (Williamson et al., 1986; Boslough et al., 1986; Boslough, 1991). Pyrrhotite, a possible carrier of Martian magnetic anomalies, has only recently received attention (Rochette et al., 2003; Louzada et al., 2005).

The study of magnetic properties under static pressure has benefited from refined experimental techniques such as reversible magnetic susceptibility measurements of micron-sized samples in diamond anvil cells (Gilder et al., 2002) and neutron diffraction under pressure (Rochette et al., 2003). However, we do not have a clear picture of the behavior of magnetic remanence under nonhydrostatic conditions such as impacts. Natural settings such as impact craters and nuclear explosion test sites (e.g., Hargraves and Perkins, 1969) lack precise pressure calibration and may be too complex for isolating the effect of the numerous parameters involved (i.e., rheology, magnetic mineralogy, preexisting magnetization, temperature). Shocks simulated by explosives (Martelli and Newton, 1977; Srnka et al., 1979; Pesonen et al., 1997) also lack precise pressure calibration and magnetic field control (Soloviev and Sweeney, 2005). Most early experiments that used aluminum (Hornemann et al., 1975; Cisowski and Fuller, 1978) or copper projectiles (Dickinson and Wasilewski, 2000) to simulate hypervelocity impacts were not accurately calibrated and were destructive. Brecciation caused by the impact (e.g., Pohl et al., 1975) can limit the maximum pressure reached by these experiments. However, modern mechanical impact experiments using gas or powder guns can recover intact samples with good pressure calibration (e.g., Louzada et al., 2005).

In this paper we propose a new approach for studying impact magnetization by combining laser impacts and room-temperature scanning Superconducting Quantum Interference Device (SQUID) microscopy.

## METHODS OF INVESTIGATION

### Laser Impact

High-power pulsed lasers focused on spots a few millimeters in diameter are widely used to generate high-pressure shocks as high as hundreds of GPa into materials. This technique is of particular interest for the study of geological materials under planetary impact conditions. Laser shocks generate pressures similar to those occurring during an impact of a small body onto a planetary surface, although with much shorter duration, allowing the recovery of the samples and quenching of high-pressure shock defects (Langenhorst et al., 2002).

We used an Nd-glass laser, which had a wavelength of 1.06 μm, a pulse intensity with a Gaussian temporal variation (25 ns duration at half maximum), and a maximum available energy of 25 J. The laser was fired through a layer of water at two separate locations on the top surface of a cylindrical basalt core (diameter 25 mm, height 22 mm). By focusing the laser on a spot several millimeters in diameter at the surface of the sample, the high-intensity irradiation ($>1 GWcm^{-2}$) produces a dense plasma a few microns thick whose expansion induces a shock wave that propagates

© 2006 Geological Society of America. For permission to copy, contact Copyright Permissions, GSA, or editing@geosociety.org.

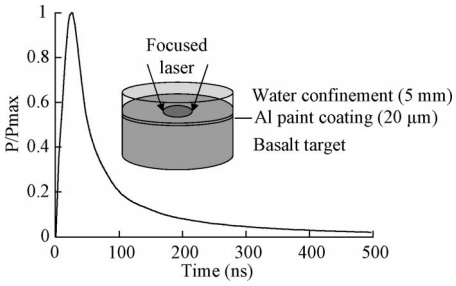


**Figure 1. Experimental setup for shock generation by water-confined laser irradiation and pressure (*P*) loading history (normalized to peak pressure) of sample surface during laser irradiation.**

in the sample. Water is transparent to the laser and amplifies both the pressure and duration by confining the plasma produced by the laser at the surface of the sample. A thickness of ~5 mm of water is used to avoid any parasitic reverberation at the free surface of the water that could alter the mechanical loading induced by the plasma expansion. In order to better control the pressure wave driven into the sample, the core was coated with ~20 μm of aluminum paint prior to shocking. The shock is therefore generated by the expansion of the aluminum plasma, which allows us to use the pressure calibration (i.e., the shock amplitude for a given laser irradiation) derived under similar experimental conditions for pure aluminum targets (Berthe et al., 1997). This shock amplitude is applied to a normalized time history shock profile calculated with a simple absorption model (Romain and Auroux, 1997) using a 25 ns Gaussian laser pulse and water confinement.

As the material compression is followed by a release wave a few nanoseconds later, the initial shock amplitude decays while the shock propagates inside the target. Hence, there is a gradient in peak pressure with depth in the sample. In order to characterize this pressure vs. depth relationship, we computed two-dimensional axisymmetric simulations with the Radioss finite element code (Boustie and Cottet, 1991) (www.radioss.com) using an elasto-plastic constitutive law for basalt with the Mie Grüneisen equation of state (which relates energy to pressure and volume), the Hugoniot (which relates pressure and volume), and the applied pressure profile given in Figure 1. The Hugoniot curve was determined using experimental data. The parameters used for the simulation are listed in Data Repository Table DR1[1].

[1]GSA Data Repository item 2006069, Table DR1, Figures DR1–DR3, and modeling videos, is available online at www.geosociety.org/pubs/ft2006.htm, or on request from editing@geosociety.org or Documents Secretary, GSA, P.O. Box 9140, Boulder, CO 80301, USA.

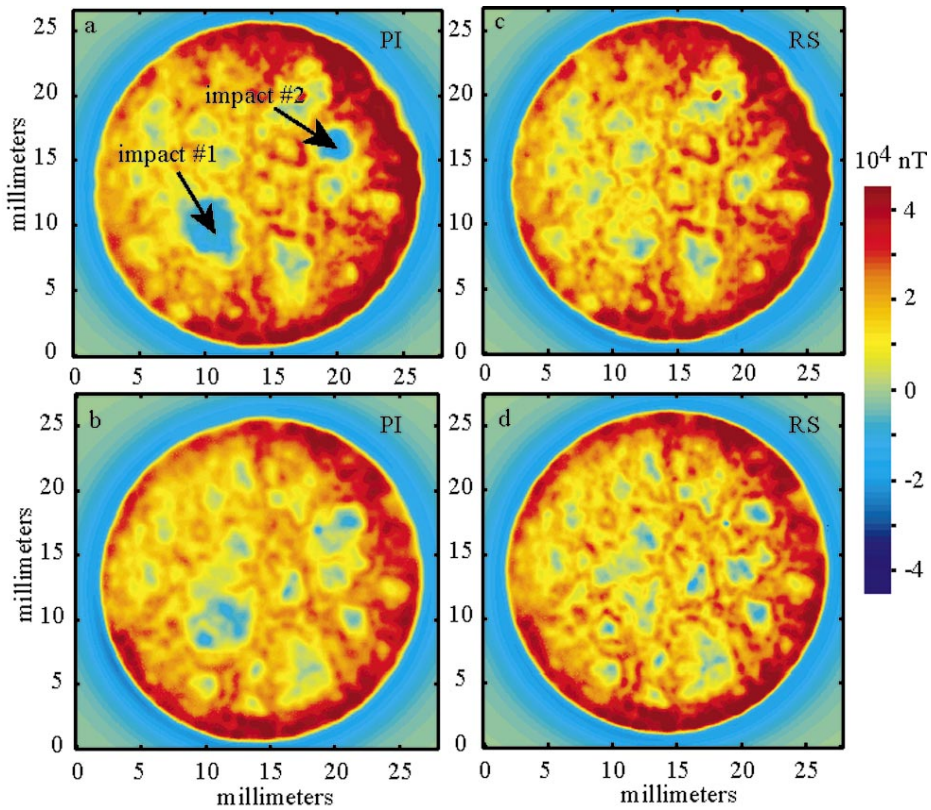


**Figure 2. Vertical component of magnetic field measured ~100 μm above sample surface. A and B: After magnetic saturation, impact, and subsequent AF demagnetization at 30 mT. C and D: After magnetic resaturation and subsequent AF demagnetization at 30 mT (A and C: upper slice; B and D: lower slice). Assuming that shock did not dramatically change rock magnetic properties of slices, images C and D represent magnetization in slices immediately before shock.**

## SQUID Microscopy

The magnetic measurements were performed with a new high-resolution scanning SQUID microscope system (described in Baudenbacher et al., 2003; Fong et al., 2005). Similar SQUID microscope systems with several times less spatial resolution have been used in a variety of previous paleomagnetic studies (Weiss et al., 2000, 2001, 2002). The new instrument uses a monolithic directly coupled low-transition-temperature niobium-based planar SQUID sensor with a field sensitivity of ~1.4 pT $Hz^{-1/2}$ at frequencies greater than a few hertz. The sensor is located inside the evacuated space of a dewar and separated from the room-temperature sample by a 25-μm-thick sapphire window, allowing us to achieve sensor-to-sample distances of ~100 μm. The sensor therefore maps the perpendicular component of the magnetic field of samples with 100 μm spatial resolution. To eliminate near DC and high-frequency background noise, the whole system is housed inside a three-layer μ-metal magnetically shielded room (ambient field <100 nT).

## EXPERIMENTS ON MAGNETITE-BEARING BASALT

Our sample comes from an Oligocene basalt flow from the Ethiopian traps, described in Rochette et al. (1998). Hysteresis properties (coercivity $B_c$ = 7 mT, coercivity of remanence $B_{cr}$ = 18 mT, and S ratio $S_{300} = -0.97$) and thermomagnetic measurements (Curie temperature $T_c$ = 245 °C; Fig. DR1 [see footnote 1]) show that titanomagnetite (TM: $[Fe_3O_4]_{(1-x)}[Fe_2TiO_4]_x$ with x = 0.46) is the major ferromagnetic mineral. Hysteresis parameters (saturation remanence $M_r$ = 2.23 $10^{-1}$ $Am^2kg^{-1}$, saturation magnetization $M_s$ = 1.7 $Am^2kg^{-1}$) indicate pseudo-single domain crystals with diameters from 1 to 15 μm (Dunlop and Özdemir, 1997). The saturation magnetization value indicates a TM concentration of 4.3 wt%. The basalt core was given a saturation isothermal remanent magnetization (IRM) in a magnetic field of 3 T parallel to the core axis. It was subsequently impacted by two laser shots with energy fluxes of 6 $GWcm^{-2}$ (spot 1) and 14 $GWcm^{-2}$ (spot 2) over circular spots of diameter 4 mm and 2.5 mm, respectively (Fig. DR2). These correspond to maximum pressures of 3.5 GPa and 5 GPa. The thermal effect of such laser shots is limited to the first few tens of micrometers (Sollier, 2002).

After the impacts, two 1-mm-thick slices were cut from the core with a wire saw. The slices were three-axis AF demagnetized at 30

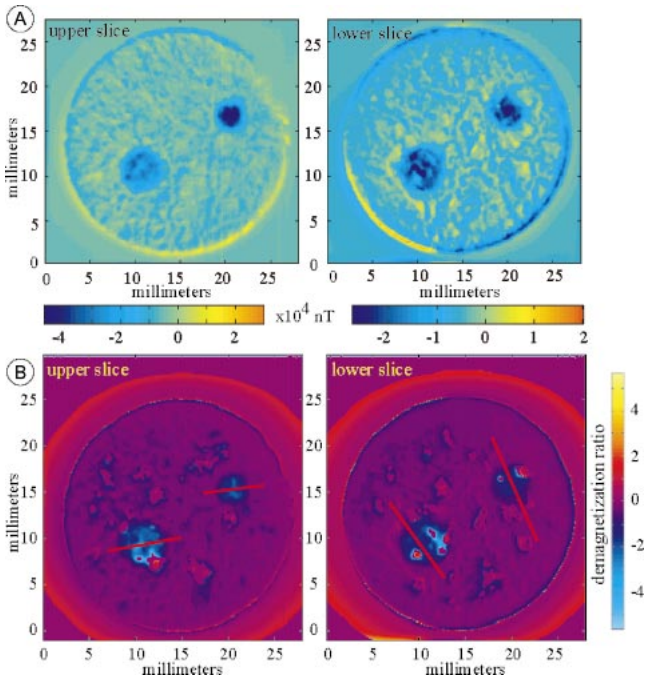


**Figure 3. A: Difference between postimpact and resaturated images (PI-RS) for upper and lower slices. The two impacted spots clearly stand out as zones with PI-RS < 0 (i.e., demagnetized). Change in sign around edge of lower slice likely results from fact that sample was slightly tilted (~0.02°) with respect to sensor during one of two scans. B: Demagnetization ratio for two slices ρ = (RS-PI)/RS. This ratio is undefined for pixels in RS that equal zero, and is meaningless for pixels in RS with very small values. We arbitrarily set ρ = 0 in those regions in RS image that have intensities <5% of maximum intensity pixel in RS. Straight lines in this image demonstrate locations of transects in Figure 4.**

mT to erase any remagnetization that may have been imparted during transport, manipulation, and sawing. This should have removed any possible IRM due to the magnetic field generated by the plasma produced by the laser (Crawford and Schultz, 1988), although such a magnetic field should have been negligible at the pressures of our experiments. An additional benefit of this treatment is that residual IRM after 30 mT AF demagnetization is a better analog for thermoremanence (TRM) than total IRM, as demonstrated by the similar behavior of TRM and residual IRM under AF demagnetization above 30 mT (Fig. DR3).

SQUID microscope measurements, called here postimpact (PI) images, were performed on the shocked slices. Measurements were also performed after the shocked slices were saturated again (and three-axis AF demagnetized at 30 mT), referred to as resaturation (RS) images. Figure 2 displays the PI and RS images. Excepting the impacted areas, the background magnetization pattern remains remarkably identical. The patchy structures observed throughout the sample correspond to the heterogeneous distribution of TM grains at the 0.1–1 mm scale.

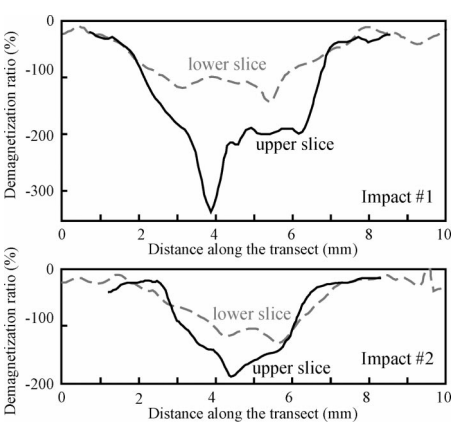


**Figure 4. Demagnetization transects across two impacts. Transect locations are shown in Figure 3.**

## DISCUSSION

The subtraction of the PI images from the RS images serves to take into account the natural background magnetic heterogeneity of the sample. The demagnetization spots associated with both impacts are clearly brought out by this technique (Fig. 3A). In order to quantify the demagnetization process, we computed the fractional demagnetization ratio by differencing the RS and PI images normalized to the RS images, (RS-PI)/RS (Fig. 3B). This quantity is not a true estimate of demagnetization because RS and PI are in units of field rather than magnetization. Outside the impacted areas, the demagnetization is not zero, but ~20%. This is probably due to a slight variation in the sensor to surface distance between the two measurement runs.

The demagnetization ratio for the upper slice is above 100% inside the impacted areas (Fig. 4). This is expected for a nonmagnetized area within a uniformly magnetized body, as demagnetizing fields originating from the surrounding magnetized region will be oppositely oriented with respect to this magnetization in the nonmagnetized area. The same behavior is visible on the lower slice at the center of the impacted area. The transects across the upper slice show that the impacted areas are nearly

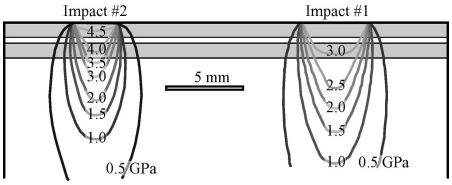


**Figure 5. Peak pressure contours in impacted basalt core derived from impact modeling. Shaded areas correspond to two studied slices.**

completely demagnetized. For the lower slice, the transition between the nondemagnetized and demagnetized areas is more gradual, as shown by the progressive diminution of the demagnetization ratio toward the center of the impacted areas. This type of magnetic anomaly profile is typical of what has been observed above lunar (Halekas et al., 2002) and Martian craters (Mohit and Arkani-Hamed, 2004).

Impact modeling provides a map of the overall sample pressure state at various times (Video DR1 and Video DR2; see footnote 1), from which we can deduce maximum peak pressure isocontours of the sample after shock propagation (Fig. 5). These isocontours of pressure can be superimposed on the demagnetization transects. In view of the small (~100 μm) sample to sensor distance during magnetic measurements, the magnetic anomalies are essentially an image of the magnetization of the upper few tens of micrometers of the studied slices. Therefore, the peak pressure contours are considered at 50 μm below the slice surface. Through this superimposition, we obtain a relation between the peak pressure undergone by the basalt and the demagnetization ratio (Fig. 6). The curves obtained from the lower slice for the two impacts are essentially identical, confirming the validity of our experimental approach. These curves do not represent the actual demagnetization of the basalt vs. pressure, since full inversion of the magnetic field data is needed to obtain the intensity of magnetization of the

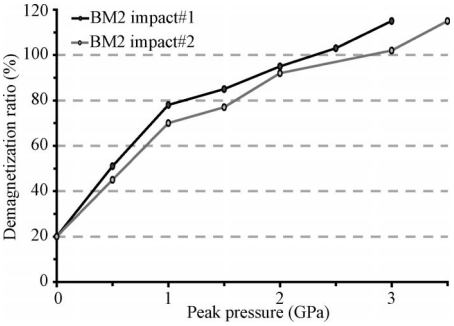


**Figure 6. Demagnetization ratio (RS-PI)/RS vs. peak pressure determined for the two impacts in lower slice. RS—resaturated, PI—postimpact.**

basalt. Nevertheless, they provide a qualitative proxy to the demagnetization of the impacted sample vs. pressure. In particular, the transects across the upper slice confirm that the basalt is already fully demagnetized at 3 GPa.

Despite the presence of an ambient field of ~50 μT during the impact experiments, nothing can be said from these experiments about the efficiency of impact remagnetization. Even if the acquisition of shock remanence was as efficient as the acquisition of TRM, the region of the sample remagnetized by the impact would only acquire a magnetization that would be a few percent of the initial saturation IRM, and would therefore appear as nearly completely demagnetized.

## CONCLUSION

We show that the combination of two innovative techniques, i.e., laser impacts and SQUID microscopy, is a powerful tool for studying remagnetization associated with natural hypervelocity impacts. A single laser impact on a given material yields a continuous relationship between the demagnetization intensity and pressure. The planned development of this methodology on samples with well-characterized magnetic properties and mineralogy, as well as experiments in a controlled, nonzero magnetic field, will provide insights into the nature of magnetic anomalies on Mars and the Moon, and the remanent magnetization of meteorites. Future improvements will include studying the effects of shock on natural remanent magnetization in controlled ambient magnetic field, measurements along the direction of the impacts (to increase the spatial resolution of the demagnetization pattern), and inversion of the magnetic field data to obtain a precise quantitative estimate of the intensity of remagnetization or demagnetization under pressure.


## ACKNOWLEDGMENTS

This study was funded by the INSU/CNES Programme de Planétologie. Weiss thanks the National Science Foundation Geophysics and the National Aeronautics and Space Administration Mars Fundamental Research Programs for their support. We thank N. Barlow, S. Stewart, and D. Dunlop for constructive reviews and are grateful to Mecalog group (Antony, France) for providing the Radioss software.


## REFERENCES CITED


Baudenbacher, F., Fong, L.E., Holzer, J.R., and Radparvar, M., 2003, Monolithic low-transition-temperature superconducting magnetometers for high resolution imaging magnetic fields of room temperature samples: Applied Physics Letters, v. 82, p. 3487–3489.

Berthe, L., Fabbro, R., Peyre, P., Tollier, L., and Bartnicki, E., 1997, Shock waves from a water-confined laser-generated plasma: Journal of Applied Physics, v. 82, p. 2826–2832.

Boslough, M.B., 1991, Shock modification and chemistry and planetary geologic processes: Annual Review of Earth and Planetary Sciences, v. 19, p. 101–130.

Boslough, M.B., Venturini, E.L., Morosin, B., Graham, R.A., and Williamson, D.L., 1986, Physical properties of shocked and thermally altered nontronite—Implications for the Martian surface: Journal of Geophysical Research, v. 91, p. E207–E217.

Boustie, M., and Cottet, F., 1991, Experimental and numerical study of laser induced spallation into aluminum and copper targets: Journal of Applied Physics, v. 69, p. 7533–7538.

Chen, G., Ahrens, T.J., and Hide, R., 1995, Hypervelocity impacts and magnetization of small bodies in the solar system: Icarus, v. 115, p. 86–96.

Cisowski, S.M., and Fuller, M., 1978, The effect of shock on the magnetism of terrestrial rocks: Journal of Geophysical Research, v. 83, p. 3441–3456.

Cisowski, S.M., Dunn, J.R., Fuller, M., YeeMing Wu, Rose, M.F., and Wasilewski, P.J., 1976, Magnetic effects of shock and their implications for lunar magnetism (II): New York, Pergamon Press, Proceedings of the 7th Lunar Science Conference, p. 3299–3320.

Crawford, D.A., and Schultz, P.H., 1988, Laboratory observations of impact-generated magnetic fields: Nature, v. 336, p. 50–52.

Dickinson, T.L., and Wasilewski, P., 2000, Shock magnetism in fine particle iron: Meteoritics and Planetary Science, v. 35, p. 65–74.

Dunlop, J.D., and Özdemir, Ö., 1997, Rock magnetism: Fundamentals and frontiers: Cambridge, Cambridge University Press, 573 p.

Fong, L.E., Holzer, J.R., McBride, K.K., Lima, E.A., and Baudenbacher, F., 2005, High resolution room-temperature sample scanning superconducting quantum interference device microscope configurable for geological and biomagnetic applications: Review of Scientific Instruments, v. 76, doi: 10.1063/1.1884025.

Fuller, M.D., 1977, Review of effects of shock (<60 kbar; $<6 \times 10^9$ Pa) on magnetism of lunar samples: Royal Society of London Philosophical Transactions, v. 285, p. 409–416.

Gilder, S.A., Le Goff, M., Peyronneau, J., and Chervin, J.C., 2002, Novel high pressure magnetic measurements with application to magnetite: Geophysical Research Letters, v. 29, doi: 10.1029/2001GL014227.

Gilder, S.A., Le Goff, M., Chervin, J.C., and Peyronneau, J., 2004, Magnetic properties of single and multi-domain magnetite under pressures from 0 to 6 GPa: Geophysical Research Letters, v. 31, doi: 10.1029/2004GL019844.

Halekas, J.S., Mitchell, D.L., Lin, R.P., Hood, L.L., Acuña, M.H., and Binder, A.B., 2002, Demagnetization signatures of lunar impact craters: Geophysical Research Letters, v. 29, doi: 10.1029/2001GL013924.

Halekas, J.S., Lin, R.P., and Mitchell, D.L., 2003, Magnetic fields of lunar multi-ring impact basins: Meteoritics and Planetary Sciences, v. 38, p. 565–578.

Hargraves, R.B., and Perkins, W.E., 1969, Investigations of the effect of shock on natural remanent magnetism: Journal of Geophysical Research, v. 74, p. 2576–2589.

Hood, L., Richmond, N.C., Pierazzo, E., and Rochette, P., 2003, Distribution of crustal magnetic fields on Mars: Shock effects of basin-forming impacts: Geophysical Research Letters, v. 30, doi: 10.1029/2002GL016657.

Hornemann, U., Pohl, J., and Bleil, U., 1975, A compressed air gun accelerator for shock magnetization and demagnetization experiments up to 20 kbar: Journal of Geophysics, v. 41, p. 13–22.

Langenhorst, F., Boustie, M., Deutsch, A., Hornemann, U., Matignon, C., Migault, A., and Romain, J.P., 2002, Experimental techniques for the simulation of shock metamorphism: A case study on calcite, *in* Davison, L., et al., eds., High pressure shock compression of solids V: Shock chemistry with applications to meteorite impacts: New York, Springer Verlag, p. 1–27.

Louzada, K., Stewart, S.T., and Weiss, B.P., 2005, Shock demagnetization of pyrrhotite: 36th Lunar and Planetary Science Conference, Houston, Texas, abs. 1134.

Martelli, G., and Newton, G., 1977, Hypervelocity cratering and impact magnetisation of basalt: Nature, v. 269, p. 478–480.

Mohit, P.S., and Arkani-Hamed, J., 2004, Impact demagnetization of the martian crust: Icarus, v. 168, p. 305–317.

Pesonen, L.J., Deutsch, A., Hornemann, U., and Langenhorst, F., 1997, Magnetic properties of diabase samples shocked experimentally in the 4.5 to 35 GPa range: 28th Lunar and Planetary Science Conference, p. 1087–1088.

Pohl, J., Bleil, U., and Hornemann, U., 1975, Shock magnetization and demagnetization of basalt by transient stress up to 10 kbar: Journal of Geophysics, v. 41, p. 23–41.

Rochette, P., Tamrat, E., Féraud, G., Pik, R., Courtillot, V., Ketefo, E., Coulon, C., Hoffmann, C., Vandamme, D., and Yirgu, G., 1998, Magnetostratigraphy and timing of the Oligocene Ethiopian traps: Earth and Planetary Science Letters, v. 164, p. 497–510.

Rochette, P., Fillion, G., Ballou, R., Brunet, F., Ouladdiaf, B., and Hood, L., 2003, High pressure magnetic transition in pyrrhotite and impact demagnetization on Mars: Geophysical Research Letters, v. 30, doi: 10.1029/2003/GL0117359.

Romain, J.P., and Auroux, E., 1997, Acceleration-deceleration process of thin foils confined in water and submitted to laser driven shocks: Journal of Applied Physics, v. 82, p. 1367–1373, doi: 10.1063/1.365913.

Soloviev, S.P., and Sweeney, J.J., 2005, Generation of electric and magnetic field during detonation of high explosive charges in boreholes: Journal of Geophysical Research, v. 110, doi: 10.1029/2004JB003223.

Srnka, L.J., Martelli, G., Newton, G., Cisowski, S.M., Fuller, M.D., and Schaal, R.B., 1979, Magnetic field and shock effects and remanent magnetization in a hypervelocity impact experiment: Earth and Planetary Science Letters, v. 42, p. 127–137.

Sollier, A., 2002, Etude des plasmas générés par interaction laser-matière en régime confiné. Application au traitement des matériaux par choc laser [Ph.D. thèse]: Versailles Saint-Quentin-en-Yvelines University, 297 p.

Wasilewski, P., 1976, Shock-loading meteoritic b.c.c. metal above the pressure transition: Remanent-magnetization stability and microstructure: Physics of the Earth and Planetary Interiors, v. 11, p. P5–P11.

Weiss, B.P., Kirschvink, J.L., Baudenbacher, F.J., Vali, H., Peters, N.T., MacDonald, F.A., and Wikswo, J.P., 2000, A low temperature transfer of ALH84001 from Mars to Earth: Science, v. 290, p. 791–795.

Weiss, B.P., Baudenbacher, F.J., Wikswo, J.P., and Kirschvink, J.L., 2001, Magnetic microscopy promises a leap in sensitivity and resolution: Eos (Transactions, American Geophysical Union), v. 82, p. 513–518.

Weiss, B.P., Vali, H., Baudenbacher, F.J., Kirschvink, J.L., Stewart, S.T., and Shuster, D.L., 2002, Records of an ancient Martian magnetic field in ALH84001: Earth and Planetary Science Letters, v. 201, p. 449–463.

Williamson, D.L., Venturini, E.L., Graham, R.A., and Morosin, B., 1986, Morin transition of shock-modified hematite: Physical Review B: Condensed Matter and Materials Physics, v. 34, p. 1899–1907.



Manuscript received 31 May 2005
Revised manuscript received 27 October 2005
Manuscript accepted 28 November 2005

Printed in USA